Article

Not peer-reviewed version

Autonomous Landing Control for Quadrotors on Wave – Excited Marine Platforms

Florin Costache * and Adrian–Mihail Stoica

Posted Date: 7 April 2026

doi: 10.20944/preprints202604.0307.v1

Keywords: backstepping control; nonlinear control; autonomous landing; UAV-marine interaction; sea-state modeling; Pierson-Moskowitz spectrum; Modified Pierson-Moskowitz spectrum; Lyapunov stability

doi:10.20944/preprints202604.0307.v1

Article

Autonomous Landing Control for Quadrotors on Wave—Excited Marine Platforms

Florin Costache [1,*] and Adrian–Mihail Stoica [2]

[1] GMV INNOVATING SOLUTIONS SRL, Calea Floreasca 246C, Sky Tower Building 32nd floor, 014476 Bucharest, Romania

[2] Faculty of Aerospace Engineering, National University of Science and Technology POLITEHNICA Bucharest, Gheorghe Polizu 1-7, 011061 Bucharest, Romania

* Correspondence: costacheflorin93@gmail.com

Abstract

A nonlinear backstepping control framework is developed for autonomous landing of a quadrotor on a wave-excited marine platform. The study addresses the underactuated nature of the aerial vehicle and the strong coupling between translational and rotational dynamics, ensuring stable trajectory tracking under sea-induced disturbances. Reference trajectories are generated through physically grounded Pierson-Moskowitz (PM) and Modified Pierson-Moskowitz (MPM) wave spectra, enabling realistic modeling of vertical heave motion, while horizontal position and yaw are defined through harmonic components adapted to the sea-state regime. The controller is designed through a seven-step recursive backstepping procedure, with Lyapunov functions guaranteeing asymptotic stability of the tracking errors for the regulated outputs. A modular MATLAB simulation platform is implemented, integrating the full 6-DOF quadrotor dynamics, the control algorithm, and spectral reference generation. Numerical simulations demonstrate that the Lyapunov function derivatives remain negative over the entire simulation horizon, confirming asymptotic convergence. Comparative results with a tuned PID (Proportional-Integral-Derivative) controller indicate superior tracking performance, damping and reduced amplitude and phase errors for the backstepping approach, especially under MPM-based trajectories representing rough sea states. The proposed framework establishes a reliable basis for adaptive extensions and future Hardware-in-the-Loop validation of autonomous landing on moving marine platforms.

Keywords: backstepping control; nonlinear control; autonomous landing; UAV-marine interaction; sea-state modeling; Pierson-Moskowitz spectrum; Modified Pierson-Moskowitz spectrum; Lyapunov stability

---

1. Introduction

Autonomous landing of unmanned aerial vehicles (UAVs) on dynamically moving platforms represents a critical challenge in modern aerospace engineering, due to intrinsic nonlinearities, underactuated structure, and strong coupling between translational and rotational dynamics. In maritime environments, these difficulties are further intensified by continuous and irregular motions of the landing platform induced by sea waves, wind, and external disturbances. Ensuring stable and accurate trajectory tracking under such conditions remains a key requirement for reliable autonomous operations.

Quadrotor-type UAVs have experienced significant growth in civil, industrial, and military applications, including surveillance, offshore logistics, infrastructure inspection, and search-and-rescue missions. Among the most demanding operational scenarios is autonomous landing on mobile platforms, where oscillatory and partially unpredictable motions impose strict constraints on control performance. Conventional control approaches often rely on simplified assumptions regarding platform motion, typically using constant or purely sinusoidal reference trajectories. While effective

Preprints.org (www.preprints.org) | NOT PEER-REVIEWED | Posted: 7 April 2026 doi:10.20944/preprints202604.0307.v1

for preliminary analysis, such representations fail to capture the stochastic and broadband nature of real sea states, limiting the realism of controller validation.

Spectral wave models, such as the Pierson-Moskowitz (PM) spectrum and its modified formulations, provide a physically grounded description of sea-surface dynamics by characterizing the distribution of wave energy across frequencies. Their use enables the generation of reference trajectories that more accurately reflect the vertical heave motion of marine platforms under different sea conditions. However, the integration of such spectral models into nonlinear UAV control frameworks remains relatively limited, particularly in the context of autonomous landing and stability-critical maneuvers.

Nonlinear control strategies offer a suitable framework for addressing these challenges. Among them, the backstepping method is well suited for underactuated systems, providing a systematic recursive design procedure and explicit stability guarantee through Lyapunov theory. Previous studies have demonstrated the effectiveness of backstepping for quadrotor stabilization and trajectory tracking. Nevertheless, its application to UAV landing on wave-excited marine platforms, combined with realistic sea-state modeling, has received comparatively limited attention.

In contrast to conventional control approaches predominantly validated for constant or weakly time-varying reference signals, the present work explicitly targets control performance under dynamic and non-stationary references representative of realistic marine environments. The specific contributions of this article include:

- Integration of physically grounded PM and MPM wave spectra into the reference generation process, enabling assessment of controller performance beyond idealized deterministic inputs and emphasizing the advantages of nonlinear control in stochastic excitation regimes;
- Design of a nonlinear backstepping controller with explicit Lyapunov-based stability guarantees for the coupled translational and rotational dynamics of the UAV;
- Systematic validation of the backstepping control method for time-varying reference signals, showing superior damping characteristics, reduced phase and amplitude errors, and improved robustness when tracking broadband, sea-spectrum-based trajectories;
- Development of a modular MATLAB-based simulation platform enabling systematic performance evaluation, gain sensitivity analysis, and comparison with a conventional PID controller;
- Demonstration of the limitations of classical PID control in the presence of non-constant reference trajectories, where phase lag, amplitude distortion, and oscillatory transients become significant under sinusoidal and wave-induced motions;
- Quantitative gain sensitivity analysis highlights the ability of the backstepping framework to maintain stability and tracking accuracy across a wide range of dynamic operating conditions, where linear controllers exhibit degraded performance.

The paper is organized as follows: the next section presents the dynamic model of the UAV and the design methodology for the backstepping controller considering the interaction between the autonomous UAV and the marine vessel. The third section presents numerical simulation results for the verification and validation of the nonlinear controller performances in comparison with the ones obtained in the linear design framework. These results are analyzed and discussed in Section 4. The paper ends with some concluding remarks.

2. Backstepping Controller Design for the UAV – Marine Interaction

This section describes the modeling assumption, reference generation, control design, and numerical setup required for the nonlinear control algorithms and their implementation, verification and validation presented in the next sections.

 doi:10.20944/preprints202604.0307.v1

2.1. Quadrotor Modeling and Reference Frames

A quadrotor UAV is modeled as a rigid body with six degrees of freedom (6-DOF) and four control inputs (see e.g., [1–3]). The following two reference frames are considered [4]:

- Inertial frame E^a $(O^a, \overrightarrow{e_1^a}, \overrightarrow{e_2^a}, \overrightarrow{e_3^a})$: fixed to the ground, used to express position and Euler angles;
- Body-fixed frame E^m $(O^m, \overrightarrow{e_1^m}, \overrightarrow{e_2^m}, \overrightarrow{e_3^m})$-attached to the UAV, used to express forces, moments, and body velocities.

The translational position of the center of mass is denoted by $\zeta \triangleq [x, y, z]^T$, while the attitude is described by Euler angles $\eta \triangleq [\phi, \theta, \psi]^T$ (roll, pitch, yaw). The kinematic relations are expressed through transformation matrices $R_t(\phi, \theta, \psi)$ and $R_r(\phi, \theta)$ linking inertial derivatives to body-fixed linear and angular velocities [4]:

- $\dot{\zeta} = R_t V$;
- $\Omega = R_r \dot{\eta}$,

where V and Ω are the body-fixed translational and angular velocity vectors, respectively.

The dynamic equations follow Newton-Euler rigid-body mechanics, including gravity and aerodynamic drag:

- Translational dynamics include thrust contribution and linear drag K_t;
- Rotational dynamics include rotor-induced moments, gyroscopic/aerodynamic damping K_r, and inertia coupling through $I_T = diag\left(I_x, I_y, I_z\right)$.

The propulsion system is modeled through individual rotor thrusts F_i, $i \in \{1, \dots, 4\}$, producing the total thrust and the body moments. The model is underactuated (6 outputs, 4 inputs). The controlled outputs are selected as x, y, z, ψ, while ϕ, θ are stabilized indirectly through the hierarchical control structure.

2.2. Structured State Representation for Backstepping

To apply recursive backstepping control design methodology adopted in this paper, the state variables are grouped into structured channels [4]:

- $x_1 = [x\ y]^T$, $x_2 = [\dot{x}\ \dot{y}]^T$;
- $x_3 = [\phi\ \theta]^T$, $x_4 = \left[\dot{\phi}\ \dot{\theta}\right]^T$;
- $x_5 = [\psi\ z]^T$, $x_6 = \left[\dot{\psi}\ \dot{z}\right]^T$;
- $x_7 = [F_1\ F_2\ F_3\ F_4]^T$.

Following the notations from [4], the dynamics are separated into three subsystems (translation-attitude coupling, yaw-altitude, rotor dynamics), written in a compact nonlinear form using drift terms f_0, f_1, f_2, input gains g_0, g_1, g_2, and auxiliary mappings ϕ_0, ϕ_1, ϕ_2, consistent with standard backstepping formulations for underactuated multirotor.

$$S_1: \begin{cases} \dot{x_1} = x_2 \\ \dot{x_2} = f_0(x_2, x_3, x_5, x_6) + g_0(x_5, x_7)\varphi_0(x_3) \\ \dot{x_3} = x_4 \\ \dot{x_4} = f_1(x_3, x_4, x_6, x_7) + g_1(x_3)\varphi_1(x_7) \end{cases} \tag{1}$$

$$S_2: \begin{cases} \dot{x_5} = x_6 \\ \dot{x_6} = f_2(x_3, x_4, x_6, x_7) + g_2(x_3)\varphi_2(x_7) \end{cases} \tag{2}$$

$$S_3: \dot{x_7} = u \tag{3}$$

where matrices g_0, g_1, g_2 have the following expressions

$$g_0 = \frac{\sum_{i=1}^{4} F_i}{m} \begin{bmatrix} sin\psi & cos\psi \\ -cos\psi & sin\psi \end{bmatrix},\ g_1 = \begin{bmatrix} \frac{1}{I_x} & \frac{1}{I_y} sin\phi\ tan\theta \\ 0 & \frac{1}{I_y} cos\phi \end{bmatrix},\ g_2 = \begin{bmatrix} \frac{1}{I_z} cos\phi \frac{1}{cos\theta} & 0 \\ 0 & \frac{1}{m} cos\phi\ cos\theta \end{bmatrix} \tag{4}$$

and with the vectors ϕ_0, ϕ_1, ϕ_2 given by:

Preprints.org (www.preprints.org) | NOT PEER-REVIEWED | Posted: 7 April 2026 doi:10.20944/preprints202604.0307.v1

$$\varphi_0 = \begin{bmatrix} sin\phi \\ cos\phi\ sin\theta \end{bmatrix},\ \varphi_1 = \begin{bmatrix} d(F_2 - F_4) \\ d(F_3 - F_1) \end{bmatrix},\ \varphi_2 = \begin{bmatrix} c(F_1 - F_2 + F_3 - F_4) \\ F_1 + F_2 + F_3 + F_4 \end{bmatrix},\ f_0 = \begin{bmatrix} f_x \\ f_y \end{bmatrix},\ f_1 = \begin{bmatrix} f_\phi \\ f_\theta \end{bmatrix},\ f_2 = \begin{bmatrix} f_\psi \\ f_z \end{bmatrix}, \quad (5)$$

in which:

$$\begin{bmatrix} f_x \\ f_y \\ f_z \end{bmatrix} = -\frac{1}{m} R_t K_t R_t^T \dot{\zeta} - G, \quad (6)$$

$$\begin{bmatrix} f_\phi \\ f_\theta \\ f_\psi \end{bmatrix} = -(I_T R_r)^{-1}\left[I_T\left(\frac{\partial R_r}{\partial \phi}\dot{\phi} + \frac{\partial R_r}{\partial \theta}\dot{\theta}\right)\dot{\eta} - K_r R_r \dot{\eta} - (R_r\dot{\eta}) \times (I_T R_r \dot{\eta})\right] + \begin{bmatrix} \frac{c}{I_z} cos\phi\ tan\theta \sum_{i=1}^4 (-1)^{i+1} F_i \\ -\frac{c}{I_z} sin\phi \sum_{i=1}^4 (-1)^{i+1} F_i \\ \frac{d}{I_y} sin\phi \frac{1}{cos\theta}(F_3 - F_1) \end{bmatrix} \quad (7)$$

2.3. Sea-State Modeling and Reference Trajectory Generation

Marine motion is represented through stochastic wave election synthesized as a sum of harmonic components with random phases. Sea elevation is modeled as [5]:

$$\zeta(t) = \sum_{i=0}^N \bar{\zeta}_i cos\,(\omega_i t + \theta_i) \quad (8)$$

where $\theta_i \in [-\pi, \pi]$ ensures stationarity, N is the number of spectral components, and $\bar{\zeta}_i$ is computed from the wave spectrum $S(\omega)$ over a frequency band $\Delta\omega$ [5]:

$$\bar{\zeta}_i \approx \sqrt{2\int_{\omega_i - \frac{\Delta\omega}{2}}^{\omega_i + \frac{\Delta\omega}{2}} S(\omega) d\omega}. \quad (9)$$

Two spectral models are used for the applications considered in this paper:

- Pierson-Moskowitz (PM) spectrum (fully developed sea), parametrized primarily by significant wave height $h_{1/3}$: $S_{PM}(\omega) = \frac{0.78}{\omega^5} exp\left(\frac{-3.11}{\omega^4 h_{1/3}^2}\right)$ $[m^2 s]$ (see e.g., [5,6]);
- Modified Pierson-Moskowitz (MPM) spectrum, recommended by maritime standards (12th and 15th International Towing Tank Conference – ITTC, 1969,1978, and The 2nd International Ship and Offshore Structures Congress – ISSC, 1964) for broader and more realistic frequency content, parametrized by $h_{1/3}$ and dominant period T: $S_{MPM}(\omega) = \frac{4\pi^3 h_{1/3}^2}{\omega^5 T^4} exp\left(\frac{-16\pi^3}{\omega^4 T^4}\right)$ $[m^2 s]$ ([5,7]).

Spectral energy describes the distribution of wave energy over frequency. Figure 1 compares the PM and MPM spectra for the same characteristic period $T = 7s$ and for different significant wave heights ($h_{1/3} = 2, 4, 6m$). As $h_{1/3}$ increases, the spectral energy level rises and the peak shifts toward lower frequencies, indicating that higher waves are slower and more energetic. Accordingly, the area under the spectrum – proportional to the total sea energy – increases with $h_{1/3}$ (see e.g., [5–10]).

The PM spectrum concentrates energy around a well-defined dominant frequency, representing a fully developed sea. In contrast, the MPM spectrum spreads energy over a wider frequency range, with greater low-frequency content, more realistically capturing mixed long and short-wave components. Therefore, MPM is generally preferred for rough sea simulations (as recommended by 12th and 15th International Towing Tank Conference – ITTC, 1969,1978, and The 2nd International Ship and Offshore Structures Congress – ISSC, 1964), while PM remains a reference model for fully developed sea conditions and theoretical analyses.

Preprints.org (www.preprints.org) | NOT PEER-REVIEWED | Posted: 7 April 2026 doi:10.20944/preprints202604.0307.v1

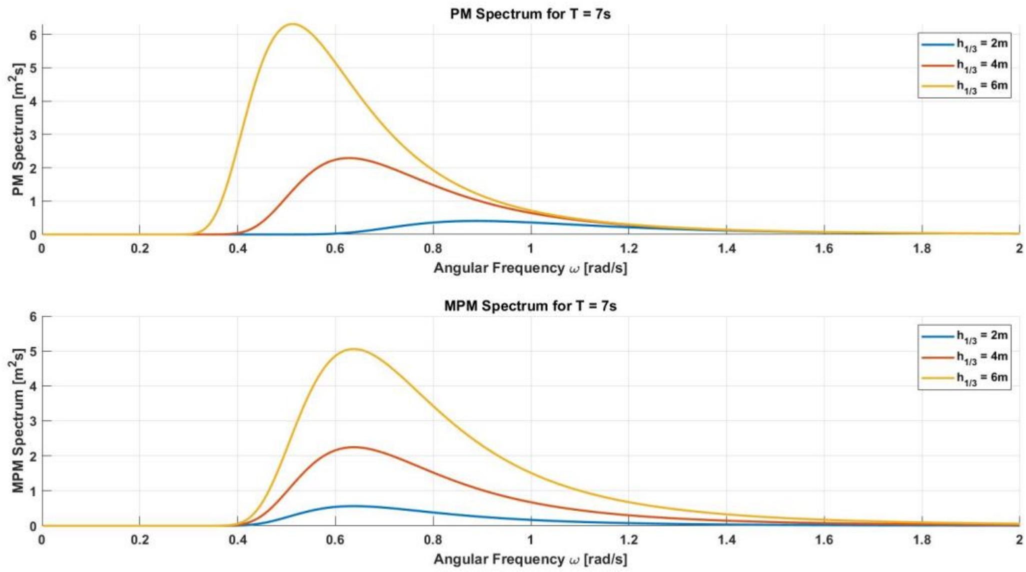

Figure 1. PM and MPM spectra recommended by ITTC and ISSC for different significant wave heights, $h_{1/3}$.

In the implemented generator, vertical reference $z_d(t)$ is produced by PM or MPM synthesis (optionally in a narrow band around the spectral peak to obtain a smoother heave). Horizontal and yaw references are defined as harmonic signals with configurable amplitude, frequency, and phase. The desired trajectory is defined by the vectors:

- $x_{1d}(t) = [x_d(t)\ y_d(t)]^T$;
- $x_{5d}(t) = [\psi_d(t)\ z_d(t)]^T$

and their time derivatives $\dot{x}_{1d}(t)$, $\dot{x}_{5d}(t)$, generated analytically for the harmonic components and numerically/analytically for the spectral component depending on implementation choice.

To highlight the effects of the parameters listed in Table 1, the reference trajectories generated using the PM and MPM spectra are illustrated below. Figure 2 presents the calm sea case, while Figure 3 corresponds to rough sea conditions, for the variables $x(t), y(t), z(t), \psi(t)$.

Table 1. Input parameters for reference generation.

Component	Parameter	Value/Expression	
		Calm Sea	Rough Sea
Motion on x-axis	Amplitude A_x	2m	3.5m
	Frequency f_x	0.1Hz (period = 10s)	0.5Hz (period = 2s)
Motion on y-axis	Amplitude A_y	2m	3.5m
	Frequency f_y	0.1Hz (period = 10s)	0.5Hz (period = 2s)
Yaw ψ	Amplitude A_ψ	±2° (≈ 0.035rad)	±5° (≈ 0.052rad)
	Frequency f_ψ	0.1Hz (period = 10s)	0.5Hz (period = 2s)
Altitude z (PM)	Model	Pierson-Moskowitz	Pierson-Moskowitz
	Significant height $h_{1/3}$	2m	4m
	Components N	100	100
Altitude z (MPM)	Model	Modified Pierson-Moskowitz	Modified Pierson-Moskowitz
	Parameters	$h_{1/3}$ = 2m, T = 8s, N = 100	$h_{1/3}$ = 4m, T = 10s, N = 100

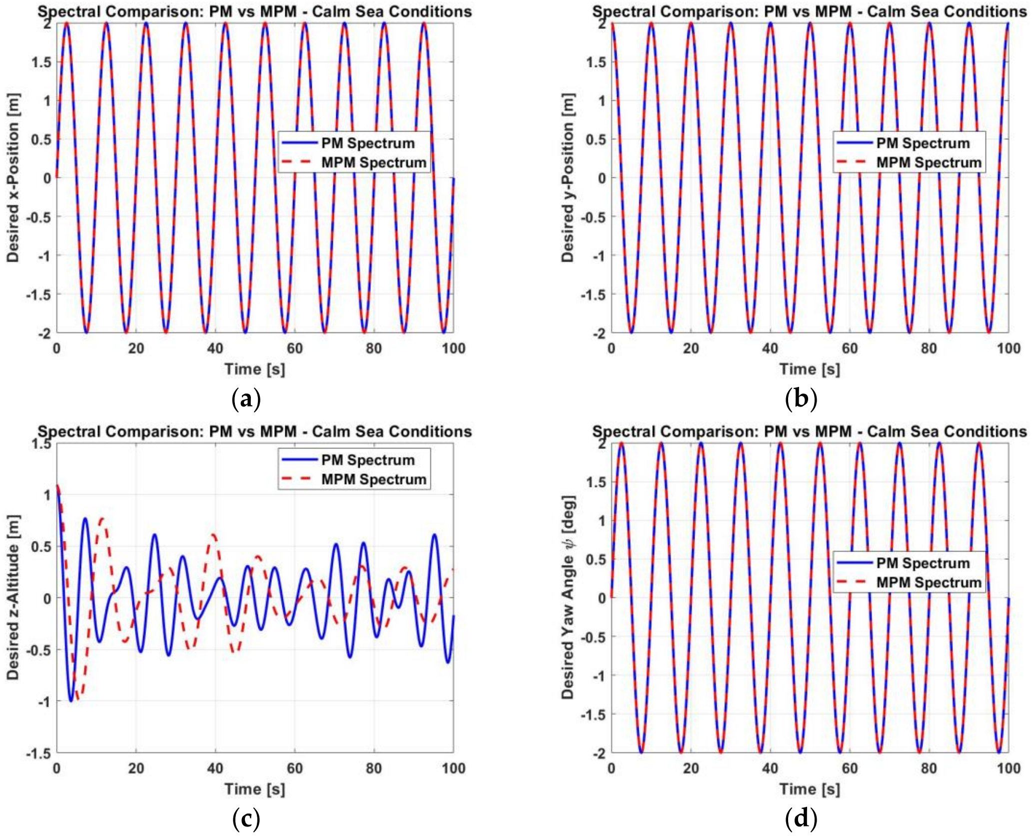

Figure 2. Calm Sea PM vs. MPM comparison: (**a**) Desired x-Position vs time, (**b**) Desired y-Position vs time, (**c**) Desired z-Position vs time, (**d**) Desired Yaw Angle vs time.

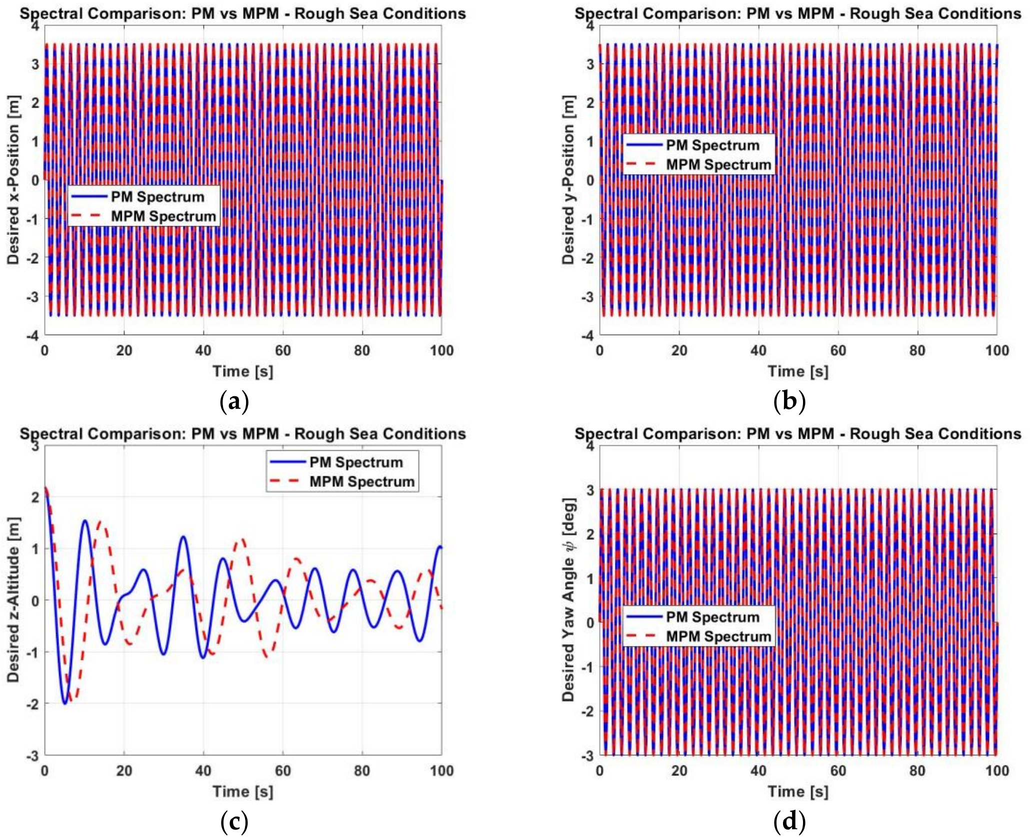

Figure 3. Rough Sea PM vs. MPM comparison: (**a**) Desired x-Position vs time, (**b**) Desired y-Position vs time, (**c**) Desired z-Position vs time, (**d**) Desired Yaw Angle vs time.

Reproducibility is ensured through an optional deterministic random seed applied to the phase vector θ. Multi-directional effects are introduced through an optional propagation direction parameter χ and evaluation point (X_0, Y_0) in the phase argument.

2.4. Backstepping Controller Design

Based on the structured state representation for the backstepping procedure as presented in Section 2.2, a seven-step recursive backstepping controller is implemented for the selected regulated outputs x, y, z, ψ ([4]).

Step 1. *For the first step the virtual system is considered* $\dot{x_1} = v_1$. *Let the first tracking error* $z_1 = x_{1d} - x_1$ *and consider the Lyapunov function positive definite* $V_1 = \frac{1}{2} z_1^T z_1$. *Its time derivative is* $\dot{V_1} = z_1^T \dot{z_1} = z_1^T(\dot{x_{1d}} - \dot{x_1}) = z_1^T(\dot{x_{1d}} - v_1)$. *The stabilization of* z_1 *can be obtained by introducing a first virtual control input* $v_1 = A_1 z_1 + \dot{x_{1d}}$, *with* $A_1 \in \mathbb{R}^{2x2}$ *is a positive definite matrix. The Lyapunov time derivative is then* $\dot{V_1} = -z_1^T A_1 z_1 < 0$ *[4].*

Step 2: *For the second step, the following new virtual system is considered* $\dot{x_2} = f_0(x_2, x_3, x_5, x_6) + g_0(x_5, x_7) v_2$, *where* v_2 *is a second virtual control input. The variable change is introduced by making* $z_2 = v_1 - x_2 = A_1 z_1 + \dot{x_{1d}} - \dot{x_1}$ *(where* $\dot{z_1} = \dot{x_{1d}} - \dot{x_1}$ *), hence* $\dot{z_1} = -A_1 z_1 + z_2$. *For the second step, the augmented Lyapunov function is considered* $V_2 = \frac{1}{2} \sum_{i=1}^{2} z_i^T z_i$. *Its time derivative is*

$$\dot{V_2} = z_1^T \dot{z_1} + z_2^T \dot{z_2} = z_1^T(-A_1 z_1 + z_2) + z_2^T(\dot{v_1} - \dot{x_2}) = -z_1^T A_1 z_1 + z_2^T(z_1 + \dot{v_1} - f_0 - g_0 v_2).$$

The stabilization of z_2 *can be obtained by introducing the following augmented virtual control* $v_2 = g_0^{-1}(z_1 + A_2 z_2 + \dot{v_1} - f_0)$ *with* $A_2 \in \mathbb{R}^{2x2}$ *is a positive definite matrix.*

Remark 1: It is worth noting that the determinant of the matrix g_0 *is* $\left(\frac{1}{m} \sum_{i=1}^{4} F_i\right)^2 > 0$, *if* $\sum_{i=1}^{4} F_i \neq 0$. *Therefore, the matrix* g_0 *is nonsingular in general operation condition because* $\sum_{i=1}^{4} F_i$ *represents the total thrust on the body in the z-axis and is generally nonzero to overcome the gravity. Therefore,* $\dot{V_2} = -\sum_{i=1}^{2} z_i^T A_i z_i < 0$ *[4].*

Step 3: *For the third step the virtual system is considered* $\dot{x_3} = v_3$. *Let*

$$z_3 = v_2 - \varphi_0(x_3) = g_0^{-1}(z_1 + A_2 z_2 + \dot{v_1} - f_0) - \varphi_0(x_3)$$

then $g_0 z_3 = z_1 + A_2 z_2 + \dot{v_1} - g_0 \varphi_0$ *(where* $\dot{z_2} = \dot{v_1} - g_0 \varphi_0$*), hence* $\dot{z_2} = -z_1 - A_2 z_2 + g_0 z_3$. *For the third step, the Lyapunov function is considered* $V_3 = \frac{1}{2} \sum_{i=1}^{3} z_i^T z_i$. *The derivative with respect to time is*

$$\dot{V_3} = z_1^T \dot{z_1} + z_2^T \dot{z_2} + z_3^T \dot{z_3} = z_1^T(-A_1 z_1 + z_2) + z_2^T(-z_1 - A_2 z_2 + g_0 z_3) + z_3^T(\dot{v_2} - \dot{\varphi_0}) = -z_1^T A_1 z_1 - z_2^T A_2 z_2 + z_3^T(g_0^T z_2 + \dot{v_2} - J_0 v_3),$$

where J_0 *is the Jacobian matrix of* φ_0 *such as* $J_0 = \frac{\partial \varphi_0(x_3)}{\partial x_3} = \begin{bmatrix} cos\phi & 0 \\ -sin\phi\ sin\theta & cos\phi\ cos\theta \end{bmatrix}$.

Remark 2: It should be noted that the determinant of the Jacobian matrix $J_0(x_3)$ *is* $cos^2\phi\, cos\theta$. *Therefore,* $J_0(x_3)$ *is non-singular when* $\phi \in \left(-\frac{\pi}{2}, \frac{\pi}{2}\right)$ *and* $\theta \in \left(-\frac{\pi}{2}, \frac{\pi}{2}\right)$, *which is generally satisfied. The stabilization of* z_3 *can be obtained by introducing a virtual control* $v_3 = J_0^{-1}(g_0^T z_2 + A_3 z_3 + \dot{v_2})$ *with* $A_3 \in \mathbb{R}^{2x2}$ *is a positive definite matrix. Then,* $\dot{V_3} = -\sum_{i=1}^{3} z_i^T A_i z_i < 0$ *[4].*

Step 4: *The final virtual system of the underactuated subsystem* S_1 *is considered* $\dot{x_4} = f_1(x_3, x_4, x_6, x_7) + g_1(x_3) v_4$. *Putting* $z_4 = v_3 - x_4 = J_0^{-1}(g_0^T z_2 + A_3 z_3 + \dot{v_2}) - x_4$, *it is obtained* $J_0 z_4 = g_0^T z_2 + A_3 z_3 + \dot{v_2} - J_0 x_4$ *(where* $\dot{z_3} = \dot{v_2} - J_0 x_4$*), hence* $\dot{z_3} = -g_0^T z_2 - A_3 z_3 + J_0 z_4$. *The global Lyapunov function of the subsystem* S_1 *is chosen as* $V_4 = \frac{1}{2} \sum_{i=1}^{4} z_i^T z_i$. *Its time derivative is*

$$\dot{V_4} = z_1^T \dot{z_1} + z_2^T \dot{z_2} + z_3^T \dot{z_3} + z_4^T \dot{z_4} = z_1^T(-A_1 z_1 + z_2) + z_2^T(-z_1 - A_2 z_2 + g_0 z_3) + z_3^T(-g_0^T z_2 - A_3 z_3 + J_0 z_4) + z_4^T(\dot{v_3} - \dot{x_4}) = -z_1^T A_1 z_1 - z_2^T A_2 z_2 - z_3^T A_3 z_3 + z_4^T(J_0^T z_3 + \dot{v_3} - f_1 - g_1 v_4).$$

The stabilization of subsystem S_1 *can be obtained by introducing the following virtual control law* $v_4 = g_1^{-1}(J_0^T z_3 + A_4 z_4 + \dot{v_3} - f_1)$, *with* $A_4 \in \mathbb{R}^{2x2}$ *is a positive definite matrix.*

Remark 3: Since the condition $\phi \in \left(-\frac{\pi}{2}, \frac{\pi}{2}\right)$ *is generally satisfied, the matrix* g_1 *is nonsingular. While replacing the control* v_4 *equation in* $\dot{V_4}$ *equation, it is obtained* $\dot{V_4} = -\sum_{i=1}^{4} z_i^T A_i z_i < 0$. *Consequently, the subsystem* S_1 *is asymptotically stable with virtual control inputs* v_1, v_2, v_3 *and* v_4.

Step 5: *In this step, the virtual system is considered* $\dot{x_5} = v_5$. *Let the tracking error* $z_5 = x_{5d} - x_5$ *and the Lyapunov function* $V_5 = \frac{1}{2} z_5^T z_5$. *Its time derivative is* $\dot{V_5} = z_5^T \dot{z_5} = z_5^T(\dot{x_{5d}} - \dot{x_5}) = z_5^T(\dot{x_{5d}} - v_5)$. *The* *stabilization of z_5 can be obtained by introducing a virtual control $v_5 = A_5 z_5 + \dot{x}_{5d}$, with $A_5 \in \mathbb{R}^{2x2}$ is a positive definite matrix. Therefore, $\dot{V}_5 = -z_5^T A_5 z_5 < 0$.*

Step 6: *For this step, the following system is defined $\dot{x}_6 = f_2(x_3, x_4, x_6, x_7) + g_2(x_3) v_6$. Let $z_6 = v_5 - x_6 = A_5 z_5 + \dot{x}_{5d} - \dot{x}_5$ (where $\dot{z}_5 = \dot{x}_{5d} - \dot{x}_5$), then $\dot{z}_5 = -A_5 z_5 + z_6$. The augmented Lyapunov function for this step is $V_6 = \frac{1}{2}(z_5^T z_5 + z_6^T z_6)$. Its time derivative is $\dot{V}_6 = z_5^T \dot{z}_5 + z_6^T \dot{z}_6 = z_5^T(-A_5 z_5 + z_6) + z_6^T(\dot{v}_5 - \dot{x}_6) = -z_5^T A_5 z_5 + z_6^T(z_5 + \dot{v}_5 - f_2 - g_2 v_6)$. The stabilization of S_2 can be obtained by introducing the following virtual control $v_6 = g_2^{-1}(z_5 + A_6 z_6 + \dot{v}_5 - f_2)$, with $A_6 \in \mathbb{R}^{2x2}$ is a positive definite matrix. Remark 4: Knowing that $\phi \in \left(-\frac{\pi}{2}, \frac{\pi}{2}\right)$ and $\theta \in \left(-\frac{\pi}{2}, \frac{\pi}{2}\right)$, it is easy to show that the matrix g_2 is nonsingular. Replacing the virtual control v_6 equation in $\dot{V}_6$ equation, it is obtained $\dot{V}_6 = -z_5^T A_5 z_5 - z_6^T A_6 z_6 < 0$. Concluding that the subsystem S_2 is asymptotically stable [4].*

Step 7: *For the final step, the propeller subsystem is defined $\dot{x}_7 = u$. Let*

$$z_7 = \begin{bmatrix} v_4 - \varphi_1(x_7) \\ v_6 - \varphi_2(x_7) \end{bmatrix} = \begin{bmatrix} g_1^{-1}(J_0^T z_3 + A_4 z_4 + \dot{v}_3 - f_1 - g_1 \varphi_1) \\ g_2^{-1}(z_5 + A_6 z_6 + \dot{v}_5 - f_2 - g_2 \varphi_2) \end{bmatrix}$$

where $\dot{z}_4 = \dot{v}_3 - f_1 - g_1 \varphi_1$ and $\dot{z}_6 = \dot{v}_5 - f_2 - g_2 \varphi_2$, hence $\dot{z}_4 = g_1^* z_7 - J_0^T z_3 - A_4 z_4$ and $\dot{z}_6 = g_2^* z_7 - z_5 - A_6 z_6$, in which $g_1^* = [g_1, O_{2x2}]$ and $g_2^* = [O_{2x2}, g_2]$ with O_{2x2} is a null matrix in $\mathbb{R}^{2x2}$. Consider the Lyapunov function candidate of the whole system $\{S_1, S_2, S_3\}$ is $V_7 = \frac{1}{2}\sum_{i=1}^{7} z_i^T z_i$. Its time derivative is given by

$$\begin{aligned} \dot{V}_7 = \sum_{i=1}^{7} z_i^T \dot{z}_i &= z_1^T(-A_1 z_1 + z_2) + z_2^T(-z_1 - A_2 z_2 + g_0 z_3) + z_3^T(-g_0^T z_2 - A_3 z_3 + J_0 z_4) \\ &+ z_4^T(-J_0^T z_3 - A_4 z_4 + g_1^* z_7) + z_5^T(-A_5 z_5 + z_6) + z_6^T(-z_5 - A_6 z_6 + g_2^* z_7) \\ &+ z_7^T\left(\begin{bmatrix} \dot{v}_4 \\ \dot{v}_6 \end{bmatrix} - \begin{bmatrix} \dot{\varphi}_1 \\ \dot{\varphi}_2 \end{bmatrix}\right) = -\sum_{i=1}^{6} z_i^T A_i z_i + z_7^T\left(\begin{bmatrix} g_1 & O_{2x2} \\ O_{2x2} & g_2 \end{bmatrix}^T \begin{bmatrix} z_4 \\ z_6 \end{bmatrix} + \begin{bmatrix} \dot{v}_4 \\ \dot{v}_6 \end{bmatrix} - \begin{bmatrix} J_1 \\ J_2 \end{bmatrix} \dot{x}_7\right) \end{aligned}$$

where $J_1 = \frac{\partial \varphi_1(x_7)}{\partial x_7}$ and $J_2 = \frac{\partial \varphi_2(x_7)}{\partial x_7}$ are the Jacobian matrices of φ_1 and φ_2 such as $J_1 = \begin{bmatrix} 0 & d & 0 & -d \\ -d & 0 & d & 0 \end{bmatrix}$, $J_2 = \begin{bmatrix} c & -c & c & -c \\ 1 & 1 & 1 & 1 \end{bmatrix}$. Therefore, the stabilization of the whole system can be obtained by introducing the following control law $u = \begin{bmatrix} J_1 \\ J_2 \end{bmatrix}^{-1}\left(\begin{bmatrix} g_1 & O_{2x2} \\ O_{2x2} & g_2 \end{bmatrix}^T \begin{bmatrix} z_4 \\ z_6 \end{bmatrix} + \begin{bmatrix} \dot{v}_4 \\ \dot{v}_6 \end{bmatrix} + A_7 z_7\right)$ with $A_7 \in \mathbb{R}^{4x4}$ is a positive definite matrix.

Remark 5: It should be noted that the determinant of the matrix $\begin{bmatrix} J_1 \\ J_2 \end{bmatrix}$ is $8cd^2$. Therefore, this matrix is nonsingular when $c > 0$ and $d \neq 0$. While replacing u equation in $\dot{V}_7$ equation, one obtains $\dot{V}_7 = -\sum_{i=1}^{7} z_i^T A_i z_i < 0$. Consequently, the whole system is asymptotically stable with the following control law [4]:

$$u = \begin{bmatrix} J_1 \\ J_2 \end{bmatrix}^{-1}\left(\begin{bmatrix} g_1 & O_{2x2} \\ O_{2x2} & g_2 \end{bmatrix}^T \begin{bmatrix} v_3 - x_4 \\ v_5 - x_6 \end{bmatrix} + \begin{bmatrix} \dot{v}_4 \\ \dot{v}_6 \end{bmatrix} + A_7 \begin{bmatrix} v_4 - \varphi_1 \\ v_6 - \varphi_2 \end{bmatrix}\right) \tag{10}$$

$$v_1 = A_1(x_{1d} - x_1) + \dot{x}_{1d} \tag{11}$$

$$v_2 = g_0^{-1}[(x_{1d} - x_1) + A_2(v_1 - x_2) + \dot{v}_1 - f_0] \tag{12}$$

$$v_3 = J_0^{-1}[g_0^T(v_1 - x_2) + A_3(v_2 - \varphi_0) + \dot{v}_2] \tag{13}$$

$$v_4 = g_1^{-1}[J_0^T(v_2 - \varphi_0) + A_4(v_3 - x_4) + \dot{v}_3 - f_1] \tag{14}$$

$$v_5 = A_5(x_{5d} - x_5) + \dot{x}_{5d} \tag{15}$$

$$v_6 = g_2^{-1}[(x_{5d} - x_5) + A_6(v_5 - x_6) + \dot{v}_5 - f_2] \tag{16}$$

2.5. Actuator Constraints: Saturation and Rate Limiting

To emulate physical rotor limitations and avoid non-physical thrust commands, constraints are imposed on:

- Rotor thrust bounds: $F_i \in [F_{min}, F_{max}]$;
- Thrust rate limits: $\dot{F}_i \in [-\dot{F}_{max}, \dot{F}_{max}]$.

The implemented logic applies:

 doi:10.20944/preprints202604.0307.v1

1. Rate limiting on $u = \dot{F}$;
2. Projection logic to prevent further decrease when F_i is at F_{min} and $u_i < 0$, and to prevent further increase when F_i is at F_{max} and $u_i > 0$.

These constraints are essential for numerical stability and for preventing unrealistic actuator behavior during aggressive transients.

2.6. PID Baseline Controller for Comparative Evaluation

A conventional PID controller is implemented as a baseline, tuned for the same plant model and evaluated under identical initial conditions and reference trajectories [11,12]. The comparison focuses on tracking quality and transient behavior under slow/fast sinusoidal references and under sea-state references generated from PM/MPM spectra. PID limitations for strongly coupled nonlinear underactuated systems are assessed primarily through overshoot, persistent oscillations, and phase lag relative to the reference.

2.7. Numerical Integration and Simulation Setup

Simulations are carried out in MATLAB R2020a using numerical integration of the nonlinear state equations. The implementation supports [13–15]:

- Adaptive integration via ode45 (Runge-Kutta) for full-model simulation;
- Fixed-step Runge-Kutta IV (as an alternative configuration) when strict sampling is required for discrete differentiation of virtual control derivatives.

Initial conditions are selected to represent a displaced state (non-zero position and yaw), while rotor thrusts are initialized uniformly around the hover equilibrium $F_1(0) = mg/4$. Nominal parameters include mass, inertias, arm length, aerodynamic drag matrices, and gravitational acceleration.

2.8. Performance Metrics and Stability Verification

Controller performance is evaluated using:

- Tracking accuracy in steady and dynamic regimes (relative error bounds);
- Response time and overshoot on selected channels;
- Amplitude error and phase error for sinusoidal references (computed from time-domain tracking signals via peak-to-peak comparison and phase shift estimation);
- Lyapunov verification: time histories of $\dot{V}$ (or stepwise components such as $\dot{V}_1$, $\dot{V}_5$) are computed and checked for negativity over the simulation horizon, providing numerical confirmation of asymptotic convergence consistent with the control design.

2.9. Availability of Code, Data, and Protocols

The computational framework is implemented as a modular MATLAB package (22 .m files). The package contains all functions required to reproduce the figures: dynamic model, reference generation (PM/MPM), control laws, Lyapunov computations, and post-processing scripts. No external datasets or accession numbers are applicable because all reference trajectories are synthetically generated from stated parametric models. Ethical approval is not applicable because the study does not involve human or animal subjects.

3. Numerical Results

Numerical simulation campaigns were conducted to evaluate tracking performance and stability of the proposed seven-step backstepping controller under representative reference scenarios, including constant references, slow/fast sinusoidal trajectories, and sea-state-inspired trajectories generated from Pierson-Moskowitz (PM) and Modified Pierson-Moskowitz (MPM) spectra. The quadrotor model and controller parameters follow Section 2, with nominal values $m = 2kg$, $I_x =$

$I_y = \frac{I_z}{2} = 1.2416 Nms^2/rad$, $d = 0.2m$, $c = 0.01m$, $g = 9.81 m/s^2$, $K_t = diag(10^{-2}, 10^{-2}, 10^{-2})$, and $K_r = diag(10^{-3}, 10^{-3}, 10^{-3})$. Rotor thrusts were initialized uniformly at hover equilibrium, $x_7(0) = mg/4[1,1,1,1]^T$. The proposed control law requires knowledge of the time derivatives of the vertical vectors $\dot{v}_1$, $\dot{v}_2$, $\dot{v}_3$, $\dot{v}_4$, $\dot{v}_5$, $\dot{v}_6$. To avoid analytical difficulties, these derivatives have been estimated numerically using a finite-difference approximation $\dot{v}_i = \frac{\Delta v_i}{\Delta t}, i = 1, \dots, 6$, where Δv_i represents the variation of v_i with respect to the previous time step, and Δt is the simulation time step [4].

Across all scenarios, stability was assessed through the time evolution of Lyapunov-related quantities computed during simulation. In addition, sensitivity to the control gain selection was evaluated by varying the diagonal matrices $A_1 \in \mathbb{R}^{2x2}, A_5 \in \mathbb{R}^{2x2}$, which directly govern convergence speed and damping in the horizontal (x, y) and (ψ, z) channels [4].

3.1. Stability Verification via Lyapunov Functions

The numerical validation confirms that Lyapunov functions associated with the selected controlled outputs remain negative over the simulation horizon, consistently supporting asymptotic convergence of tracking errors. In particular, the derivatives linked to the position and yaw-altitude channels (e.g., $\dot{V}_1$ and $\dot{V}_5$) preserve negative values throughout all analyzed scenarios, indicating dissipative closed-loop behavior and stable error dynamics.

A clear correlation is observed between gain magnitude and the transient behavior:

- Small gains (e.g., $A_1 = A_5 = diag[0.5, 0.5]$) yield conservative control action with slower decay of errors and increased phase lag for time-varying references;
- Moderate gains in the range $A_1 = A_5 \in (diag[1.5, 1.5], diag[2.5, 2.5])$ yield well-damped responses and stable convergence, matching the design specifications stated previously;
- Large gains (e.g., $A_1 = A_5 > diag[3.3, 3.3]$) tend to amplify oscillatory behavior and may lead to divergent oscillations due to overcompensation, especially under fast or highly irregular references.

3.2. Tracking Performance Under Sinusoidal References

Two sinusoidal regimes were used to evaluate controller behavior under periodic references with distinct time scales.

3.2.1. Slow Sinusoidal References

For slow sinusoidal references, the most favorable compromise between response speed and damping is obtained for $A_1 = A_5 = diag[2,2]$, as presented in Figure 4. This selection yields stable tracking with reduced transient errors and limited oscillatory behavior, maintaining good synchronization with the reference trajectory.

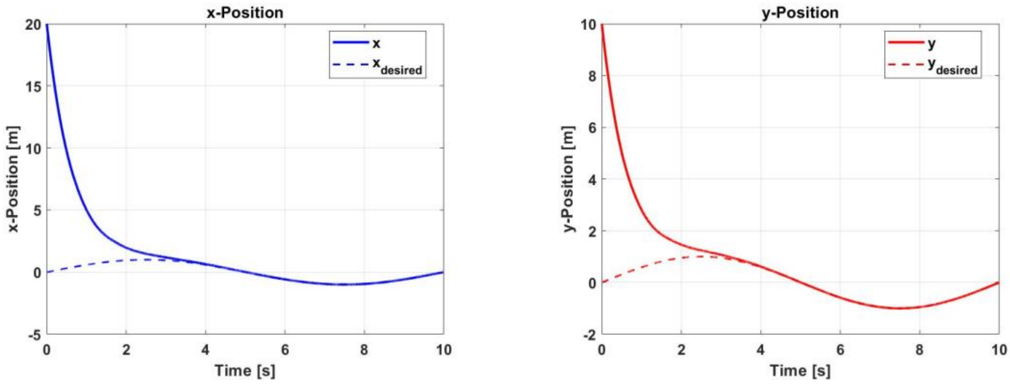

(a) (b)

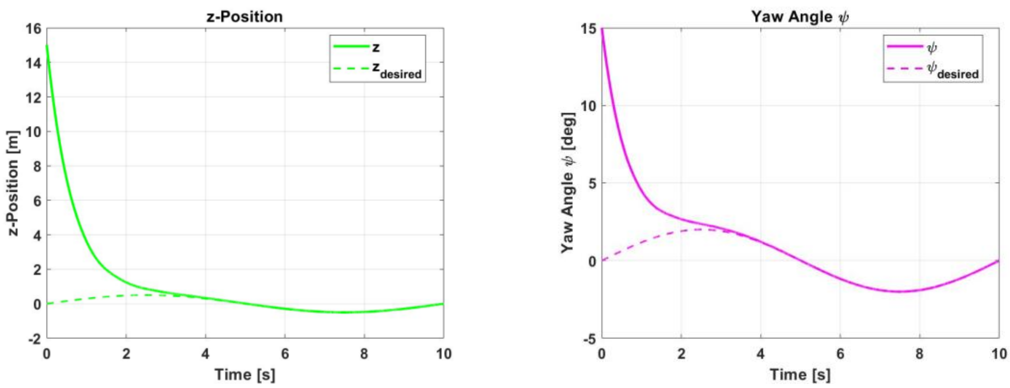

(c) (d)

Figure 4. Slow Sinusoidal Tracking Response: (a) x-Position vs time, (b) y-Position vs time, (c) z-Position vs time, (d) Yaw Angle vs time.

3.2.2. Fast Sinusoidal References

For fast sinusoidal references, improved stability and damping are achieved with slightly reduced gains $A_1 = A_5 = diag[1.5,1.5]$. Higher gains in this regime increase oscillatory response and control effort, while lower gains increase phase lag and tracking degradation. The selected value maintains stability while preserving acceptable tracking accuracy, as shown in Figure 5.

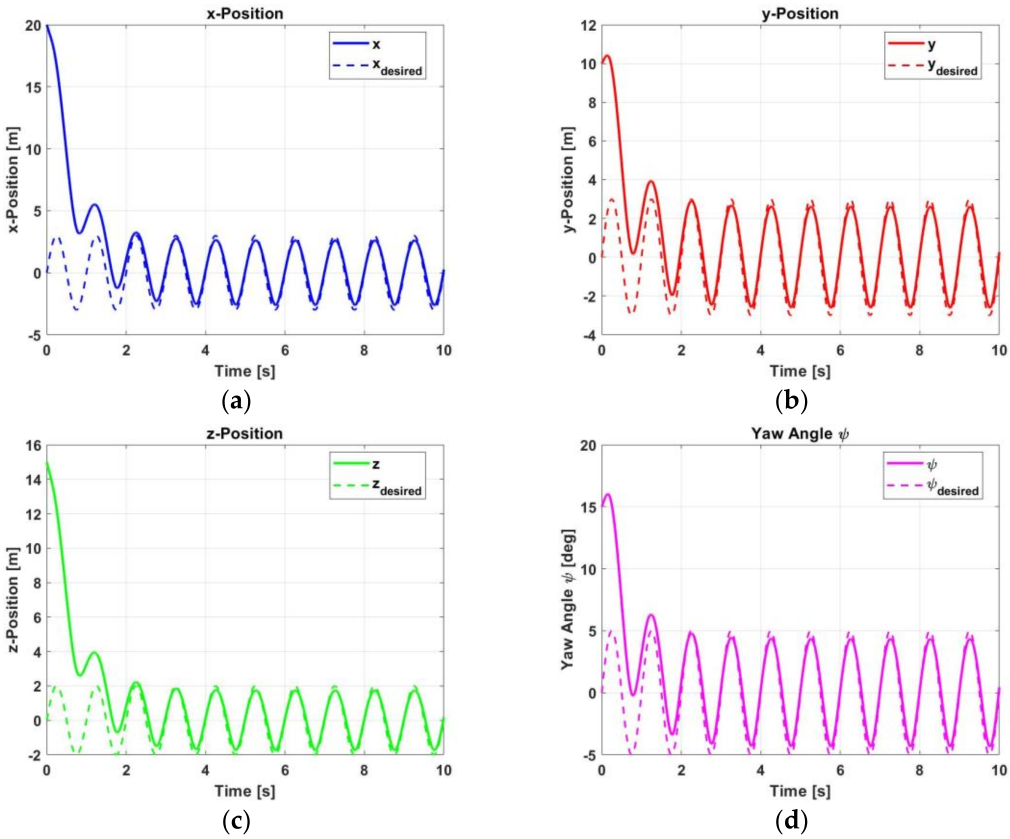

Figure 5. Fast Sinusoidal Tracking Response: (a) x-Position vs time, (b) y-Position vs time, (c) z-Position vs time, (d) Yaw Angle vs time.

3.3. Sea-State-Inspired Tracking: PM vs. MPM

Sea-state references were generated using PM and MPM spectra with $N = 100$ spectral components, combined with harmonic components for horizontal motion and yaw. Two sea conditions were evaluated:

- Calm sea: $h_{1/3} = 2m, T = 8s$ (for MPM);
- Rough sea: $h_{1/3} = 4m, T = 10s$ (for MPM).

3.3.1. Calm Sea

Under calm sea conditions, the recommended gain selection is $A_1 = A_5 = diag[2,2]$, which provides stable tracking across channels while preserving damping under irregular vertical references. These results are presented in Figure 6 for PM spectrum and in Figure 7 for MPM spectrum. The MPM-based reference consistently produces a more favorable altitude-tracking behavior compared to PM, characterized by reduced phase lag and improved amplitude consistency in $z(t)$.

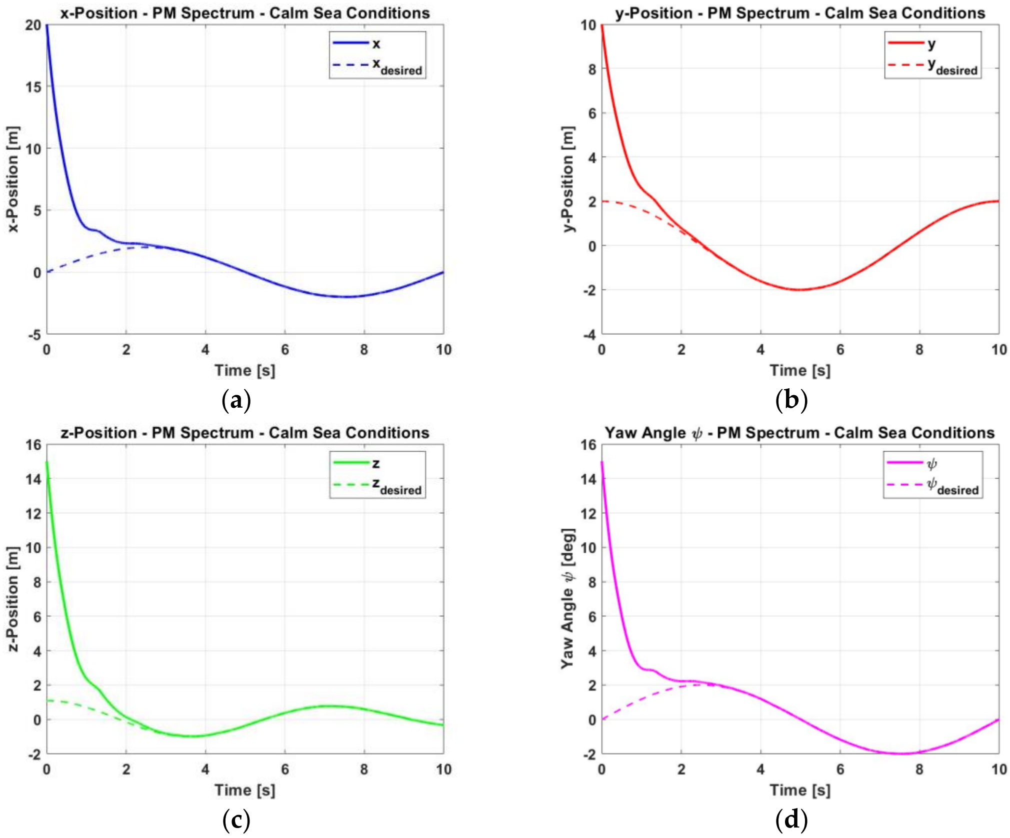

Figure 6. Calm Sea Tracking PM spectrum: (a) x-Position vs time, (b) y-Position vs time, (c) z-Position vs time, (d) Yaw Angle vs time.

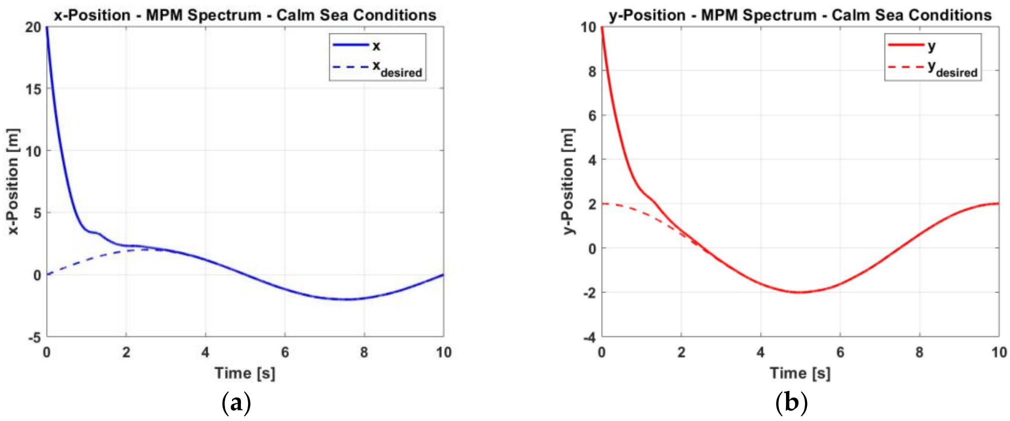

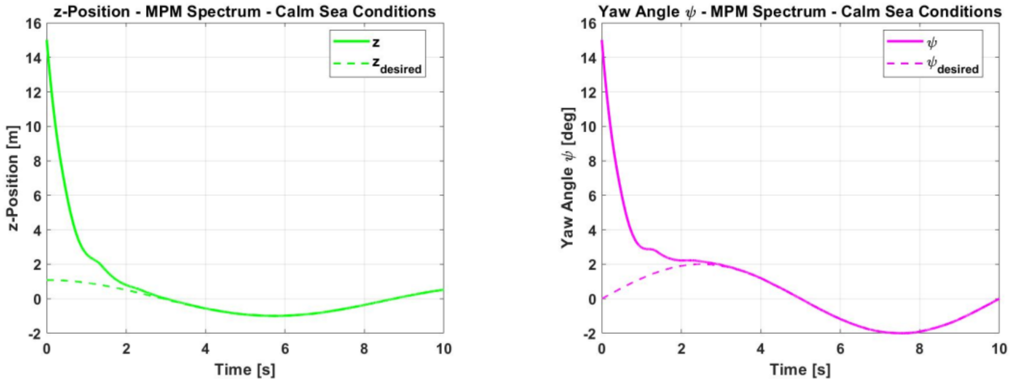

(c) (d)

Figure 7. Calm Sea Tracking MPM spectrum: (a) x-Position vs time, (b) y-Position vs time, (c) z-Position vs time, (d) Yaw Angle vs time.

3.3.2. Rough Sea

Under rough sea conditions, increased irregularity and higher energy in the heave reference produce a more demanding tracking problem. Stable performance remains attainable for moderate gains, with $A_1 = A_5 = diag[2,2]$ providing the best overall compromise in the evaluated set. These results are shown in Figure 8 for PM spectrum and in Figure 9 for MPM spectrum. Outside the moderate gain interval, two failure modes emerge: (i) divergent oscillations for large gains, and (ii) slow, inaccurate tracking for small gains. In this regime, MPM-based references again yield superior altitude tracking relative to PM, attributed to the broader spectral representation and more consistent excitation profile.

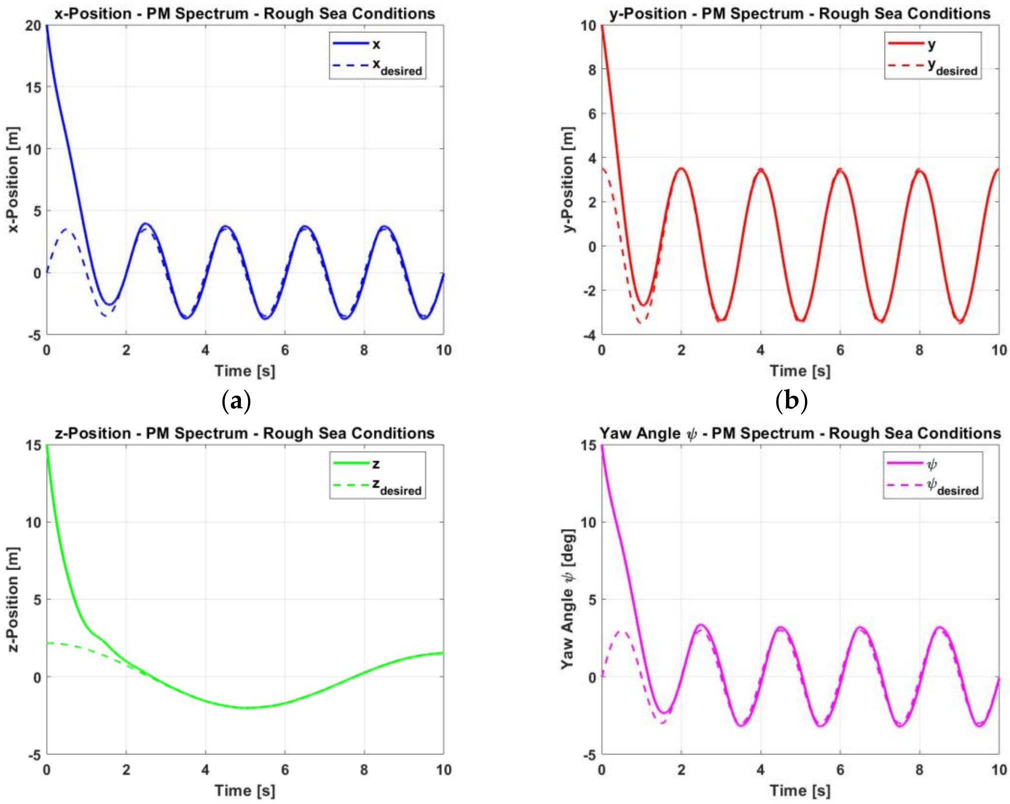

(c) (d)

Figure 8. Rough Sea Tracking PM spectrum: (a) x-Position vs time, (b) y-Position vs time, (c) z-Position vs time, (d) Yaw Angle vs time.

 doi:10.20944/preprints202604.0307.v1

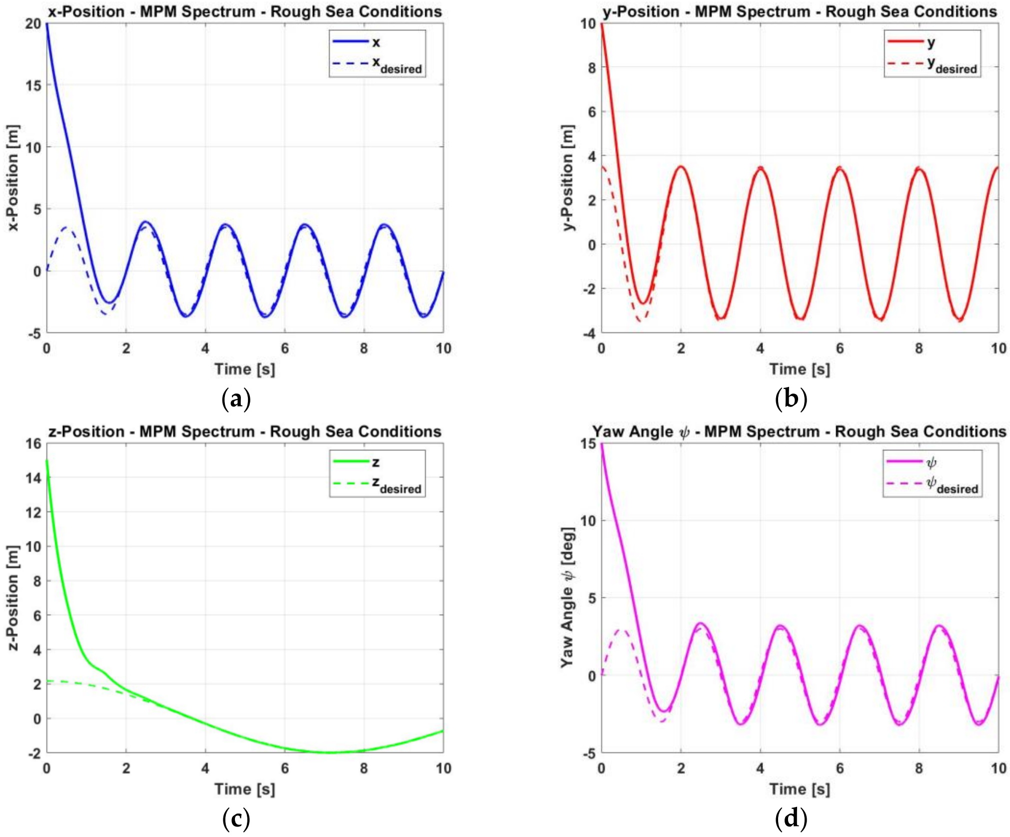

Figure 9. Rough Sea Tracking MPM spectrum: (a) x-Position vs time, (b) y-Position vs time, (c) z-Position vs time, (d) Yaw Angle vs time.

3.4. Gain Sensitivity Summary and Validated Interval

The simulations indicate that full satisfaction of the design specifications is obtained for moderate gains within $A_1 = A_5 \in (diag[1.5,1.5], diag[2.5,2.5])$. Outside this interval, tracking performance degrades markedly.

- Large values ($A_1 = A_5 > diag[3.3,3.3]$): divergent oscillations due to overcompensation;
- Small values ($A_1 = A_5 < diag[0.5,0.5]$): slow response with reduced tracking precision;
- Moderate values ($diag[1.5,1.5] \leq A_1 = A_5 \leq diag[2.5,2.5]$): best compromise between stability, accuracy, and response speed.

Table 2 summarizes the empirically recommended gain selections per scenario.

Table 2. Recommended gain values $A_1 = A_5$ across evaluated scenarios.

Scenario	Recommended $A_1 = A_5$	Observed behavior
Slow sinusoidal reference	$diag[2,2]$	Stable, well-damped tracking, reduced transient errors
Fast sinusoidal reference	$diag[1.5,1.5]$	Improved damping and stability under faster dynamics
Calm sea (PM/MPM)	$diag[2,2]$	Stable tracking; MPM improves altitude synchronization
Rough sea (PM/MPM)	$diag[2,2]$	Moderate gains required; MPM yields better altitude tracking

3.5. Backstepping vs. PID Comparative Results

Comparative simulations against a tuned PID baseline indicate consistently improved tracking under the backstepping strategy, especially for time-varying sea-state references. PID regulation maintains approximate tracking in mild regimes, but exhibits more pronounced oscillations, overshoot, and phase lag in strongly coupled and irregular scenarios (particularly for $z(t)$ and $\psi(t)$). In contrast, backstepping preserves better damping and trajectory synchronization due to its recursive structure and Lyapunov-based stabilization. The initial conditions were identical for both methods

- Initial position: $(x, y, z) = (20, 10, 15)$ m;
- Initial yaw angle: $\psi = 15°$;
- Desired state:

$$\left[x_{1_d}(t), x_{5_d}(t)\right] = \left([1sin(2\pi 0.1t), 1sin(2\pi 0.1t)]^T, [0.0349sin(2\pi 0.1t), 0.5sin(2\pi 0.1t)]^T\right),$$

where the variation in ψ corresponds to an oscillation of ± 2°. The results may be seen in Figure 10.

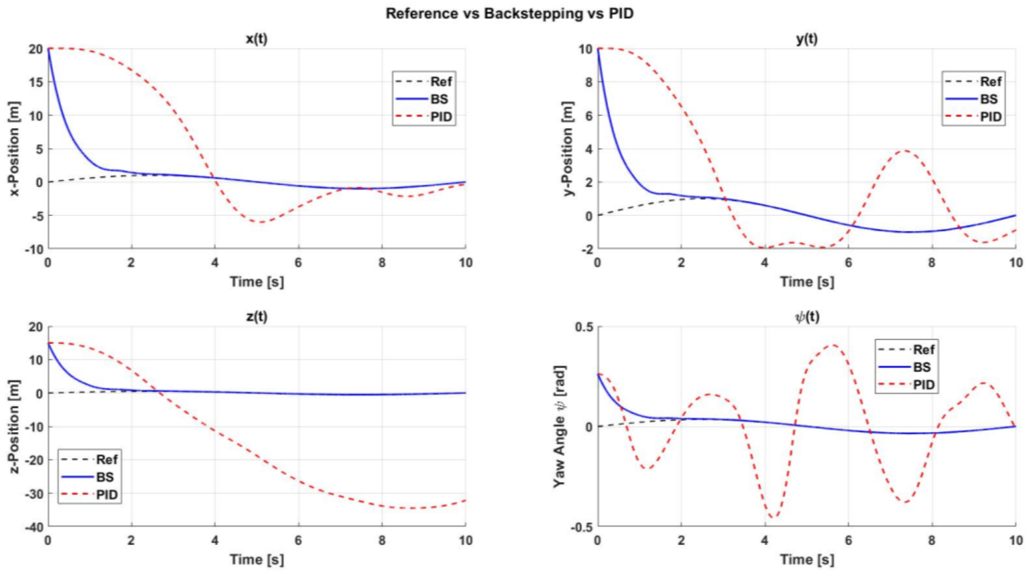

Figure 10. Backstepping vs PID.

These results confirm that the advantages of backstepping become increasingly pronounced as the reference trajectories depart from constant or purely harmonic forms.

3.6. Influence of Actuator Saturation and Rate Constraints

To evaluate the practical impact of actuator constraints introduced in Section 2.5, thrust magnitude and rate limitations were activated during all simulation campaigns. Figure 11 illustrates the time evolution of rotor thrusts $F_i(t)$, while Figure 12 presents the corresponding control rates $\dot{F}_i(t)$. The imposed constraints were $F_i \in [0.1, 12]N$, $\dot{F}_i \in [-40, 40]N/s$.

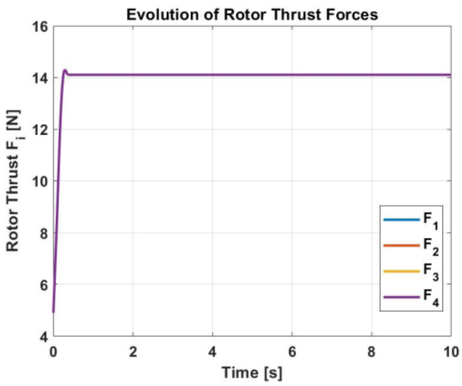

Figure 11. Time Evolution of rotor thrusts $F_1 - F_4$ under actuator saturation constraints.

Preprints.org (www.preprints.org) | NOT PEER-REVIEWED | Posted: 7 April 2026 doi:10.20944/preprints202604.0307.v1

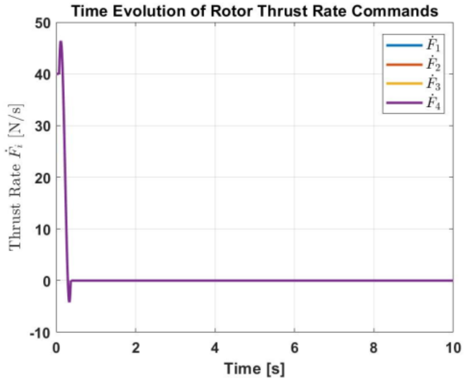

Figure 12. Time Evolution of rotor thrust rates $\dot{F}_1 - \dot{F}_4$ under rate limitation.

Quantitative analysis indicates that rate saturation was active for approximately 1.5% of the total simulation time for each rotor. These events occurred primarily during initial transients and rapid trajectory changes under rough sea conditions. For control gains within the recommended interval $A_1 = A_5 \in (diag[1.5,1.5], diag[2.5,2.5])$, the backstepping controller produced smooth thrust profiles, with limited activation of rate constraints and no sustained saturation behavior. Although transient numerical overshoots above the nominal thrust bound were observed due to numerical integration effects, however, the rate limitation mechanism prevented non-physical thrust variations and ensured bounded actuator dynamics.

These results confirm that the recursive structure of the backstepping method inherently generates smoother actuator commands, better respecting physical actuator limitations in the presence of non-constant and stochastic reference trajectories.

4. Discussion

The numerical results demonstrate that the proposed backstepping-based control framework provides a robust and theoretically consistent solution for quadrotor trajectory tracking in the presence of wave-induced marine disturbances. The persistence of negative Lyapunov function derivatives across all evaluated scenarios confirms asymptotic convergence of the tracking errors and supports the claim of global asymptotic stability for the selected controlled outputs. These findings are consistent with nonlinear control theory and validate the recursive design methodology adopted for the underactuated quadrotor system.

A distinctive contribution of this work lies in the direct integration of physically established sea-state spectral models into the control evaluation process. In contrast to many existing studies that rely on deterministic or simplified sinusoidal references, the use of Pierson-Moskowitz and Modified Pierson-Moskowitz spectra enables the generation of stochastic, frequency-rich reference trajectories that realistically emulate maritime operating conditions. This approach exposes the controller to disturbances that more closely resemble those encountered during real offshore operations and allows a more meaningful assessment of robustness and tracking performance.

The comparative analysis between PM and MPM-based references highlights that the broader spectral content of the MPM model leads to smoother altitude tracking and reduced phase lag, particularly under rough sea conditions. This observation is consistent with offshore engineering recommendations and confirms that the choice of wave spectrum has a non-negligible impact on control performance evaluation. Consequently, the proposed methodology contributes not only to control design but also to best practices in validation strategies for UAV-marine interaction problems.

Gain sensitivity studies further underline the practical relevance of the proposed framework. The existence of a well-defined interval of moderate control gains confirms that the backstepping controller exhibits predictable behavior, with a clear trade-off between convergence speed and robustness. Low gain values lead to slow dynamics and increased phase errors, whereas excessively

 doi:10.20944/preprints202604.0307.v1

large gains may induce oscillatory behavior and increased control effort. This behavior reinforces the importance of systematic gain tuning then deploying nonlinear controllers in dynamic environments.

When compared to a tuned PID controller, the backstepping approach consistently demonstrates superior damping, reduced amplitude and phase errors, and improved resilience to stochastic disturbances. These advantages stem from the explicit treatment of nonlinearities and coupling effects, as well as from the Lyapunov-based synthesis, which provides stability guarantees beyond the local operating regions typically associated with linear controllers. The results therefore extend existing comparative studies and further support the suitability of backstepping methods for autonomous landing tasks on moving platforms.

Finally, the modular MATLAB-based simulation platform represents an enabling contribution, ensuring traceability between theoretical formulations and numerical implementation. This structure facilitates reproducibility, parameter studies, and future extensions toward adaptive control strategies or Hardware-in-the-Loop validation.

Unlike conventional UAV landing studies that rely on deterministic or single-frequency references, the present framework embeds stochastic spectral sea models directly into the control validation loop, enabling stability assessment under realistic, broadband marine disturbances.

The inclusion of actuator magnitude and rate constraints provides an additional layer of realism to the control validation framework. Unlike many theoretical backstepping studies that assume unlimited actuator authority, the present implementation explicitly accounts for thrust bounds and rate saturation. The limited percentage of rate simulation (approximately 1.5%) demonstrates that the proposed controller remains largely compatible with realistic actuator dynamics. This aspect strengthens the practical relevance of the methodology and supports its potential extension toward Hardware-in-the-Loop and experimental validation.

5. Concluding Remarks

This study has presented the development and numerical validation of a nonlinear backstepping control framework for quadrotor operations in maritime environments, with particular focus on autonomous landing on moving platforms. The proposed methodology integrates rigorous mathematical modeling, Lyapunov-based control synthesis, and realistic sea-state representation within a unified simulation framework.

The derived results establish a rigorous foundation for future adaptive extensions and experimental validation, including Hardware-in-the-Loop implementation for autonomous maritime landing applications.

Author Contributions: Conceptualization, F.C. and A-M.S.; methodology, F.C. and A-M.S.; mathematical modelling, F.C. and A-M.S.; software development, F.C. and A-M.S.; numerical simulations, F.C. and A-M.S.; validation, F.C. and A-M.S.; formal analysis, F.C. and A-M.S.; investigation, F.C. and A-M.S.; visualization, F.C. and A-M.S.; writing – original draft preparation, F.C. and A-M.S.; writing – review and editing, F.C. and A-M.S.; supervision, A-M.S. All authors have read and agreed to the published version of the manuscript.

Data Availability Statement: The data presented in this study are available from the corresponding author upon reasonable request. The simulation data and MATLAB source code were generated specifically for this research and can be provided for academic and research purposes.

Acknowledgments: This work was conducted as part of doctoral research in Aerospace Engineering at the Faculty of Aerospace Engineering, National University of Science and Technology POLITEHNICA Bucharest, focusing on autonomous landing control algorithms for unmanned aerial vehicles operating on marine platforms. Academic supervision and technical discussions that contributed to the development of the control design methodology and simulation framework are gratefully acknowledged. Furthermore, this research was carried out within the framework of a national research project developed at the National Institute for Aerospace Research "Elie Carafoli" – INCAS Bucharest, entitled "Technological demonstrator for autonomous landing

 doi:10.20944/preprints202604.0307.v1

control on mobile platforms”. The project aimed at developing an integrated Hardware – In – the – Loop (HIL) simulation architecture combining real and virtual components in a unified experimental environment.

Conflicts of Interest: The authors declare no conflicts of interest. The institutional affiliations had no role in the design of the study; in the collection, analyses, or interpretation of data; in the writing of the manuscript; or in the decision to publish the results.

Abbreviations

The following abbreviations are used in this manuscript:

DOF	Degrees of Freedom
HIL	Hardware – in – the – Loop
INCAS	National Institute for Aerospace Research “Elie Carafoli”
ISSC	2nd International Ship and Offshore Structures Congress
ITTC	12th and 15th International Towing Tank Conference
MPM	Modified Pierson - Moskowitz
PID	Proportional – Integral – Derivative
PM	Pierson - Moskowitz
UAV	Unmanned Aerial Vehicle

References

1. Vukobratovic, M. Applied Dynamics of Manipulation Robots: Modelling, Analysis and Examples, Berlin: Springer-Verlag, 1989.
2. Gomes, S. B. V.; Ramos, J. G. “Airship dynamic modeling for autonomous operation,” in IEEE International Conference on Robotics and Automation, Leuven, 1998.
3. Nijmeijer, H.; Schaft, A. V. D. Nonlinear Dynamical Control Systems, New York: Springer Verlag, 1990.
4. Madani, T.; Benallegue, A. “Backstepping Control for a Quadrotor Helicopter,” in International Conference on Intelligent Robots and Systems, Beijing, 2006.
5. Perez, T.; Blanke, M. “Simulation of Ship Motion in Seaways,” 2001.
6. Price, W. C.; Bishop, R. E. Probabilistic theory of ship dynamics, London: Chapman and Hall, 1974.
7. Hervas, J. R.; Reyhanoglu, M.; Tang, H. “Automatic Landing Control of Unmanned Aerial Vehicles on Moving Platforms,” in IEEE, 2014.
8. Fossen, T. I. Handbook of Marine Craft Hydrodynamics and Motion Control, Trondheim: John Wiley & Sons Ltd., 2011.
9. Ahmad, S. Z. A. S.; Husain, M. K. A.; Zaki, N. I. M.; Mohd, M. H.; Najafian, G. “Comparison of Various Spectral Models for the Prediction of the 100-Year Design Wave Height,” International Conference on Civil, Offshore & Environmental Engineering, vol. 203, no. MATEC Web Conf., 2018.
10. Haver, S.; Moan, T. “On some uncertainties related to the short term stochastic modelling of ocean waves,” Applied Ocean Research, vol. 5, no. 2, pp. 93-108, 1983.
11. Moussid, M.; Idalene, A.; Sayouti, A.; Medromi, H. “Autonomous HexaRotor Arial Dynamic Modeling and a Review of Control Algorithms,” INTERNATIONAL RESEARCH JOURNAL OF ENGINEERING AND TECHNOLOGY, 2015.
12. Moussid, M.; Sayouti, A.; Medromi, H. “Dynamic Modeling and Control of a HexaRotor using Linear and Nonlinear Methods,” International Journal of Applied Information Systems, vol. 9, no. 5, pp. 9-17, 2015.
13. The MathWorks, Inc., “Documentation - ode45,” The MathWorks, Inc., 2025. [Online]. Available: https://www.mathworks.com/help/matlab/ref/ode45.html. [Accessed 06 06 2025].

doi:10.20944/preprints202604.0307.v1

14. Dormand, J. R.; Prince, P. J. "A family of embedded Runge-Kutta formulae," J. Comp. Appl. Math., vol. 6, pp. 19-26, 1980.
15. Shampine, L. F.; Reichelt, M. W. "The MATLAB ODE Suite," SIAM Journal on Scientific Computing, vol. 18, pp. 1-22, 1997.